Letter

Letter

Masses of neutron-rich Ni and Cu isotopes and the shell closure at Z = 28, N = 40

S. Rahaman[a], J. Hakala, V.-V. Elomaa, T. Eronen, U. Hager, A. Jokinen, A. Kankainen, I.D. Moore, H. Penttilä, S. Rinta-Antila[b], J. Rissanen, A. Saastamoinen, C. Weber, and J. Äystö

Department of Physics, University of Jyväskylä, P.O. Box 35 (YFL), FIN-40014, Finland

Abstract. The Penning trap mass spectrometer JYFLTRAP, coupled to the Ion Guide Isotope Separator On-Line (IGISOL) facility at Jyväskylä, was employed to measure the atomic masses of neutron-rich $^{70-73}$Ni and ^{73,75}Cu isotopes with a typical accuracy less than 5 keV. The mass of ^{73}Ni was measured for the first time. Comparisons with the previous data are discussed. Two-neutron separation energies show a weak subshell closure at $^{68}_{28}$Ni$_{40}$. A well established proton shell gap is observed at $Z = 28$.

PACS. 21.10.Dr Binding energies and masses – 27.50.+e $59 \leq A \leq 89$ – 27.60.+j $90 \leq A \leq 149$ – 07.75.+h Mass spectrometers

1 Introduction

Recent mass measurements on radioactive nuclei have focused on understanding the evolution of nuclear structure towards more neutron-rich nuclei. These measurements have been partly motivated by nuclear astrophysics as the rapid neutron capture process flows along the neutron-rich nuclides [1]. In addition these nuclei can be used to study nuclear-structure phenomena, such as shell-quenching, subshell closures and the evolution of the shell closures when moving towards very neutron-rich nuclei.

A subshell closure at nucleon number 40 has been studied in semidoubly-magic ^{90}Zr ($Z = 40$, $N = 50$) [2] and ^{68}Ni ($Z = 28$, $N = 40$) nuclei [3,4]. The spin-dependent neutron-proton interaction is responsible for the changes in the single-particle orbital spacings. For example, at $N = 40$, the subshell closure in ^{68}Ni originates from a relatively large spacing between the $2p_{1/2}$ and $1g_{9/2}$ neutron orbitals, but this stability effect disappears already at ^{70}Zn and ^{66}Fe which have quite low 2^+ excitation energies [5].

The $N = 40$ subshell closure has been observed to be even weaker than the $Z = 40$ subshell closure. For ^{68}Ni experimental results show contradictory evidence for the subshell closure [6–9]. The first excited state in ^{68}Ni is

a 0^+ state observed at much higher energies than the first excited states in neighbouring even-even nuclei. Also the 2^+_1 state in ^{68}Ni has a large excitation energy and the $B(E2, 0^+_{gs} \rightarrow 2^+_1)$ is quite small supporting a semidoubly-magic character of this nucleus [9]. On the other hand, observed two-neutron separation energies and shell gap energies have not shown the $N = 40$ subshell closure at $Z = 28$ [7]. Some suggested explanations are that the two-neutron separation energies are free from pairing effects, whereas pair scattering of neutrons counteracts the magicity at $N = 40$. In addition, the 2^+ excitation can be hindered by a parity change across the $N = 40$ subshell [9]. As the neutron shell gap energy of ^{68}Ni is based on the mass of ^{70}Ni known with a modest accuracy, a mass measurement of ^{70}Ni is crucial for the possible observation of the subshell closure in the neutron shell gap energies.

Another interest of the mass measurements of the nickel isotopes is triggered by the recent prediction of the tensor force calculation [10] which suggests a possible weakening of the $Z = 28$ proton shell gap beyond $N = 40$. Shell structure in the nucleus can change due to the tensor force which is a part of the meson exchange processes predicted by Yukawa [11] in nucleon-nucleon interactions. In the case of exotic nuclei, the single-particle properties can have distinct characteristics due to the tensor force [12] and the neutron-skin effect [13], that are not seen in stable nuclei. The tensor force is included in the Gogny-type mean-field model [14] (called GT2) calculations and

---

[a] e-mail: saidur.rahaman@phys.jyu.fi
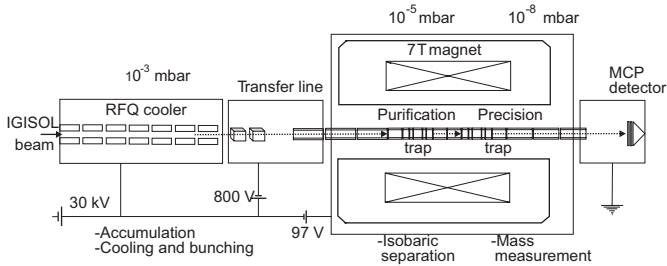[b] *Present address:* Department of Physics, University of Liverpool, Liverpool L69 3BX, UK.

Fig. 1. A schematic drawing of the JYFLTRAP setup. The Penning traps are placed inside a single 7 tesla super-conducting solenoid with two homogeneous centers.

detailed results of the single-particle energies (SPEs) for $1f_{7/2,5/2}$ and $2p_{3/2,1/2}$ for nickel isotopes are discussed in ref. [10]. The model predicts that as the neutron occupancy increases in the $1g_{9/2}$ orbital the neutron orbit stays rather constant in energy, however, the $1f_{7/2}$ and $1f_{5/2}$ proton orbits move closer to each other thus reducing the $Z = 28$ proton shell gap energy at ^{78}Ni. A precise mass value of the neutron-rich nickel isotopes can be used to test this theoretical prediction.

In this work we present precision mass data of the neutron-rich nickel and copper isotopes obtained at JYFLTRAP to probe the issues raised above. The previous direct mass measurements in this region were carried out at the time-of-flight isochronous (TOFI) spectrometer at Los Alamos [15,16] and at the Penning trap mass spectrometer ISOLTRAP at CERN, Geneva [7]. However, the large uncertainty in the mass excess of ^{70}Ni prevents a precise calculation of the neutron shell gap energy of ^{68}Ni and the pairing energy of ^{69}Ni. The masses of neutron-rich $^{70-73}$Ni and ^{73,75}Cu isotopes are presented in this work. The direct mass measurement of ^{73}Ni is reported for the first time. These mass values were used to calculate two-neutron separation, neutron shell gap and pairing energies in this region and to study the evolution of the subshell closure in ^{68}Ni and proton shell gap energies for $Z = 28$.

2 Experimental setup and analysis

JYFLTRAP [17] is an ion trap experiment for cooling, bunching, isobaric purification and precision mass measurements of radioactive ions produced at the IGISOL facility [18]. A schematic drawing of the JYFLTRAP setup is shown in fig. 1. The radioactive nuclides were produced in a proton-induced fission reaction by bombarding a natural uranium target of thickness $15 \, \text{gm/cm}^2$ with a 30 MeV proton beam from the Jyväskylä K-130 cyclotron. Radioactive ions are extracted from the gas cell by helium gas flow and guided by the sextupole ion guide (SPIG) into a differential pumping stage where they are accelerated to 30 keV and mass-separated with a 55° dipole magnet. A mass-resolving power $(M/\Delta M)$ of up to 500 can be achieved. The production rates of the studied nuclei varied from 20 ions/s to a few ions/s for the most exotic isotopes measured at a position before they enter to the radiofrequency quadrupole (RFQ) cooler and buncher.
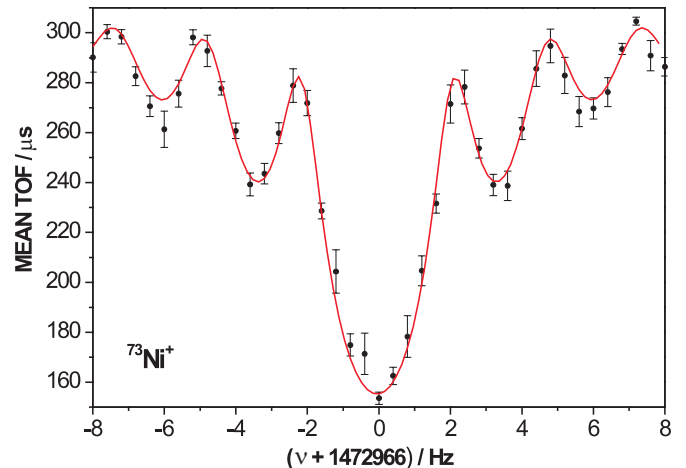

Fig. 2. Time-of-flight (TOF) resonance of ^{73}Ni$^+$ ions measured at JYFLTRAP.

In this device the ions are cooled by collisions with helium buffer gas and are accumulated at the end of the RFQ structure. The ions are extracted at low energy as a short bunch with a time structure of about $15 \, \mu s$ [19] and are injected into the purification Penning trap, where the mass selective buffer gas cooling technique is applied for further cooling and isobaric cleaning [20,21]. The mass-resolving power of the purification trap is on the order of 10^5. The purified and cooled ions are finally transported to the precision Penning trap where the cyclotron frequency (ν_c) is measured by employing the time-of-flight technique [22]. A typical time-of-flight resonance of ^{73}Ni$^+$ radioactive ions is shown in fig. 2. An excitation time $T_{ex} = 400$ ms was used in the case of ^{73}Ni and ^{73,75}Cu isotopes, whereas $T_{ex} = 800$ ms was used for $^{70-72}$Ni isotopes. The cyclotron frequency is given by

$$\nu_c = \frac{1}{2\pi} \frac{q}{m} B, \qquad (1)$$

where B is the magnetic field, m is the mass and q the charge state of the ion. To calibrate the magnetic field the cyclotron frequency $(\nu_{c,ref})$ of a precisely known reference mass (m_{ref}) is measured. The atomic mass of the ion of interest is then determined using the equation

$$m = r \cdot (m_{ref} - m_e) + m_e, \qquad (2)$$

where $r = \nu_{c,ref}/\nu_c$ is the frequency ratio and m_e is the electron mass. A typical accuracy below 5 keV has been obtained in this experiment. A detailed mass measurement procedure at JYFLTRAP can be found in refs. [23,24].

Three known systematic uncertainties were taken into account in the cyclotron frequency determinations. These are the uncertainties due to the temporal magnetic-field fluctuation, the mass difference between the reference ion to the ion of interest $m - m_{ref}$ and the frequency shift due to contaminating ions in the trap.

The linear drift of the magnetic field was taken into account by the interpolation of the reference cyclotron frequencies. In order to quantify the short temporal magnetic field fluctuations continuous cyclotron frequency

Table 1. Results from the analysis of ^{73,75}Cu and $^{70-73}$Ni measured at JYFLTRAP. The measured average frequency ratio $\bar{r}$ and its uncertainty is presented. $T_{1/2}$ represents the beta decay half-life of the studied nuclei. ME_{ex} represents the experimental mass excess obtained from the cyclotron frequency ratio. ME_{lit} are the AME03 values [25]. The last column gives the difference between the AME03 and JYFLTRAP values $\Delta = ME_{ex} - ME_{lit}$.

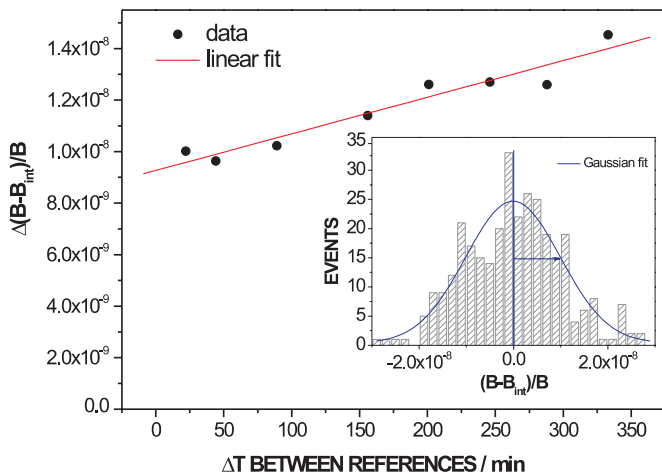| Nucleus	$T_{1/2}$/s	Freq. ratio $(\bar{r}) = \frac{\nu_c^{ref}}{\nu_c}$	ME_{ex} / keV	ME_{lit} / keV	$\Delta = ME_{ex} - ME_{lit}$ / keV
^{70}Ni	6.0	0.972 391 513(32)	−59213.8(27)	−59150(350)	−63.8
^{71}Ni	2.65	0.986 352 391(33)	−55406.2(28)	−55220(370)	−186.2
^{72}Ni	1.57	1.000 274 050(33)	−54226.0(28)	−53940(440)	−286
^{73}Ni	0.800	1.014 239 559(36)	−50108.2(31)	−49860#(300)	−248.2
^{73}Cu	1.224	1.014 107 018(34)	−58987.7(29)	−58987(4)	−0.7
^{75}Cu	4.2	1.041 982 517(35)	−54471.4(30)	−54120(980)	−351.4

Fig. 3. Relative standard deviation of the B field from the interpolated value for different time intervals ΔT between two reference measurements. This is obtained by measuring the cyclotron frequency of the ^{57}Fe$^+$ ions for 70 hours. The straight line is a linear fit to the data points. The inset presents the standard deviation of the first point.

Fig. 4. Mass excess differences between JYFLTRAP results of ^{73,75}Cu and $^{70-73}$Ni and the AME03 and TOFI values. Line values represent the JYFLTRAP results and the width of the line represents the total uncertainty. The circles and the triangles indicate the AME03 and the TOFI values with respect to the JYFLTRAP values. ^{73}Ni was measured for the first time indicated by a # mark.

measurements of stable ^{57}Fe$^+$ ions were performed for 70 hours. For the analysis the data file was subdivided into 22 minute segments. A real measurement process was simulated taking three consecutive files, the first and the third file as reference and the intermediate file as the ion of interest. The deviation of the magnetic field is obtained from the difference of the interpolated value of the cyclotron frequency ($\nu_{int} \propto B_{int}$) of the references and the measured cyclotron frequency ($\nu_m \propto B$) of the intermediate file. The standard deviation of $B - B_{int}$ is derived from the Gaussian fit to the histogram of statistical fluctuations shown in the inset of fig. 3. The standard deviation $\sigma(B - B_{int})$ as a function of the elapsed time between two references is shown in fig. 3. The uncertainty due to magnetic-field fluctuation was estimated from the linear fit to be $3.22(16) \times 10^{-11}$ /min. The offset of the linear fit was 9.2×10^{-9} and it represents the statistical uncertainty of an individual frequency measurement for ^{57}Fe$^+$ files. The count rate class and the mass-dependent systematic uncertainties were taken into account in the same way as explained in ref. [24] and references therein.
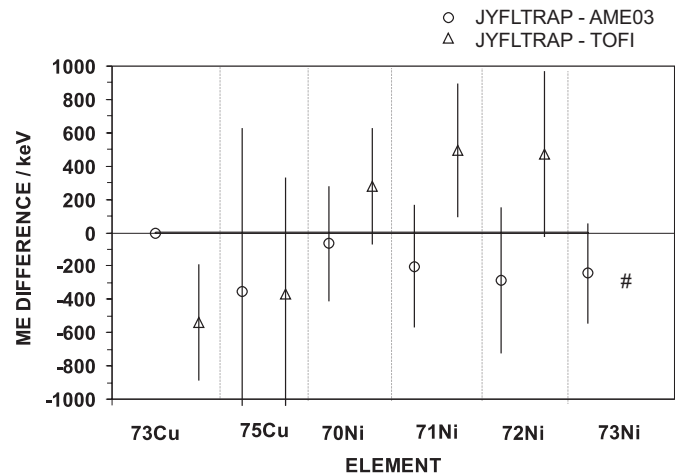
3 Results

The results of the mass measurements for ^{73,75}Cu and $^{70-73}$Ni are summarized in table 1 and discussed in the following section. The frequency ratio of each isotope is given with respect to the cyclotron frequency of the stable ^{72}Ge$^+$ isotope. The mass of the ^{72}Ge isotope is known with an uncertainty of 1.6 keV [25]. In table 1 the column ME_{ex} presents the JYFLTRAP mass excess value with the final uncertainty in parenthesis. The uncertainty contains the statistical and systematic uncertainties. Figure 4 represents the differences between the mass excess measured at JYFLTRAP and the TOFI and Atomic Mass Evaluation 2003 (AME03) values [25]. The JYFLTRAP measurements reduced the uncertainties by a factor of about 100 for each nuclei. ^{73}Ni was measured for the first time[1].

---

[1] The mass excess value of ^{73}Ni $= -48900(500)$ keV is reported in ref. [16]. However, the AME03 value claims to be an extrapolation.
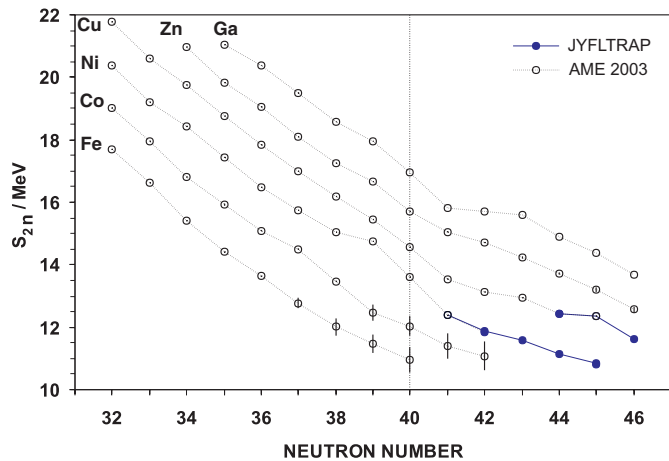
Fig. 5. S_{2n} plotted as a function of the neutron number in the region of $28 \leq N \leq 50$. The filled circles indicate the Ni and Cu isotopes from this work. A clear slope change beyond $N = 40$ is observed, separated by a vertical dotted line.

Fig. 6. S_{2n} plotted as a function of the proton number for even neutron chain. Filled circles are from this work and the empty circles are taken from the AME03. A weak irregularity is observed for $N = 40$ and 42 at $Z = 28$.

Fig. 7. S_{2p} plotted as a function of the neutron number for even proton chains. The plot is compiled from the recent JYFLTRAP and AME03 data. The AME03 extrapolated data are excluded in this plot.

In the case of the copper isotopes the AME03 and the TOFI values are shifted systematically in the same direction from the JYFLTRAP values. On the other hand, in the case of the nickel isotopes the AME03 and TOFI values are shifted from the JYFLTRAP values systematically in the opposite direction. However, the JYFLTRAP values are within the uncertainties of AME03 and TOFI values.

4 Discussion

4.1 Subshell closure at N = 40

The two-neutron separation energy S_{2n} can be obtained by using the following formula:

$$S_{2n} = -M(A, Z) + M(A - 2, Z) + 2M(1, 0), \quad (3)$$

where $M(A, Z)$ is the mass of an isotope and $M(1, 0)$ is the neutron mass. S_{2n} is shown as a function of neutron number in fig. 5 for $Z = 26$–31. The filled circles are from this work and the data are completed by the values from the AME03 [25]. Generally, S_{2n} decreases smoothly with neutron number and shell effects appear as a discontinuity. Small discontinuities are observed in the cases of ^{67,68}Ni (more bound), ^{70,71}Cu (less bound) and ^{72}Ga (less bound). Moreover, in the case of ^{68}Ni this deviation is less than 1 MeV which is rather small compared to a regular shell closure.

In fig. 5 a clear change of the slope beyond $N = 40$ is observed. This may be due to the effect of the tensor force. Filling more neutrons in the $1g_{9/2}$ orbit results in the pulling-down of the orbit. In addition as more neutrons occupy the $1g_{9/2}$ orbit the $1f_{5/2}$ and $2p_{3/2}$ orbits are crossing each other after $N = 40$. The results of these two effect may increase the S_{2n} energies, hence the slope will be reduced beyond $N = 40$.

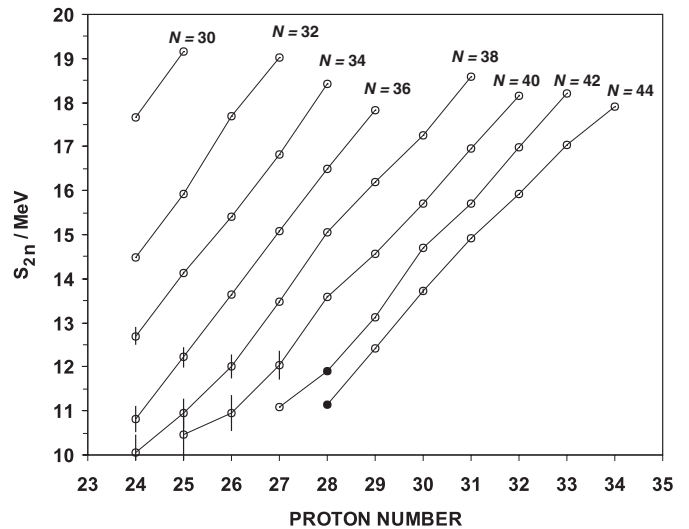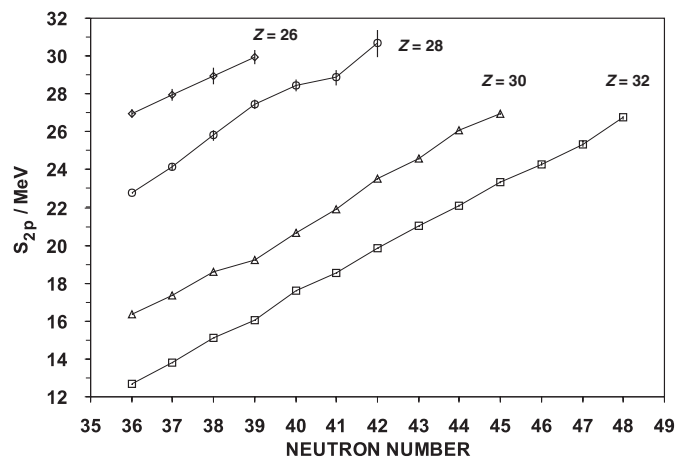Figure 6 displays S_{2n} as a function of proton number for even neutron numbers. The neutron shell gap energy is define as $\Delta(N) = S_{2n}(Z, N) - S_{2n}(Z, N + 2)$, where N defines the neutron number. The vertical distance between two consecutive isotones in fig. 6 represents the neutron shell gap energies. A small enhancement of the neutron shell gap energy at $N = 40$ for $Z = 28$ is observed but far below that expected from a shell closure. This can be explained by considering $N = 40$ as a weak subshell closure.

4.2 Proton shell gap energies for Z = 28

The two-proton separation energy S_{2p} is extracted by using the following formula:

$$S_{2p} = -M(A, Z) + M(A - 2, Z - 2) + 2M(1, 1), \quad (4)$$

where $M(1, 1)$ is the hydrogen mass. S_{2p} is plotted as a function of the neutron number in fig. 7 for even

$Z = 26$–32. In this plot the gap between the $Z = 28$ to $Z = 30$ chains yield the proton shell gap energy for $Z = 28$. The experimental data points end at $N = 41$ for the $Z = 28$ isotope chain. According to the tensor force calculations, as more neutrons are occupying $1g_{9/2}$ orbit $1f_{7/2}$ and $1f_{5/2}$ orbits are coming closer to each other resulting a reduction of the proton shell gap energy at $Z = 28$ while going from $N = 40$ to $N = 50$. In fig. 7 at $N = 41$ for $Z = 28$ a tendency of decreasing of the proton shell gap energy is noticed which is in agreement with the tensor force prediction. However, the next point at $N = 42$ has a higher shell gap energy but with a large uncertainty. This uncertainty comes from the mass of ^{68}Fe. Therefore more experimental mass data are required, in particular the masses of all n-rich Fe isotopes with reduced uncertainties to ascertain the observed trend.

5 Conclusions

In conclusion the masses of the neutron-rich nickel and copper isotopes were measured at JYFLTRAP. The mass of ^{73}Ni was measured for the first time. The shell structure around the $N = 40$ region was investigated. Precise mass values in this region are able to clarify the contradictory nature of the shell structure in ^{68}Ni. A local weak discontinuity is observed in the two-neutron separation energy for ^{68}Ni. A clear change of the slope in the two-neutron separation energy plot is observed beyond $N = 40$. A small enhancement of the neutron shell gap energy is noticed at $Z = 28$ for $N = 40$ compared to $N = 38$ and 42 which is consistent with the recent studies by other experiments [6, 9]. From these observations one can conclude that ^{68}Ni is a weak subshell closure. A detailed review of the theoretical study of shell closure and an indication of weak subshell closure is discussed in ref. [26]. A trend of the possible reduction of the proton shell gap energy is observed which is in agreement with the tensor force prediction. More experimental masses are required to be able to extract the proton shell gap energies around $Z = 28$. In the future JYFLTRAP aims to measure the masses of the neutron-rich nickel and iron isotopes to continue with this open question.

References

1. K.L. Kratz *et al.*, Z Phys. A **332**, 419 (1989).
2. L.P. Ekstrom, J. Lyttkens-Linden, Nucl. Data Sheets **67**, 579 (1992).
3. M. Bernas *et al.*, Phys. Lett. B **113**, 279 (1982).
4. R. Broda *et al.*, Phys. Rev. Lett. **74**, 868 (1995).
5. W.F. Mueller *et al.*, Phys. Rev. Lett. **83**, 3614 (1999).
6. I. Stefanescu *et al.*, Phys. Rev. Lett. **98**, 122701 (2007).
7. C. Guénaut *et al.*, Phys. Rev. C **75**, 044303 (2007).
8. K. Langanke *et al.*, Phys. Rev. C **67**, 044314 (2003).
9. O. Sorlin *et al.*, Phys. Rev. Lett. **88**, 092501 (2002).
10. T. Otsuka *et al.*, Phys. Rev. Lett. **97**, 162501 (2006).
11. H. Yukawa *et al.*, Proc. Phys. Math. Soc. Japan **17**, 48 (1935).
12. T. Otsuka *et al.*, Phys. Rev. Lett. **95**, 232502 (2005).
13. N. Fukunishi *et al.*, Phys. Rev. C **48**, 1648 (1993).
14. J. Decharge *et al.*, Phys. Lett. B **55**, 361 (1975).
15. H.L. Seifert *et al.*, Z. Phys. A **345**, 25 (1994).
16. Y. Bai *et al.*, AIP Conf. Proc. **455**, 90 (1998).
17. A. Jokinen *et al.*, Int. J. Mass Spectrom. **251**, 204 (2006).
18. J. Äystö, Nucl. Phys. A **693**, 477 (2001).
19. A. Nieminen *et al.*, Nucl. Instrum. Methods Phys. Res. B **204**, 563 (2003).
20. G. Savard *et al.*, Phys. Lett. A **158**, 247 (1991).
21. V.S. Kolhinen *et al.*, Nucl. Instrum. Methods Phys. Res. A **528**, 776 (2004).
22. M. König *et al.*, Int. J. Mass Spectrom. Ion Process. **142**, 95 (1995).
23. T. Eronen *et al.*, Phys. Lett. B **636**, 191 (2006).
24. S. Rahaman *et al.*, Eur. Phys. J. A **32**, 87 (2007).
25. G. Audi, A.H. Wapstra, C. Thibault, Nucl. Phys. A **729**, 337 (2003).
26. K. Kaneko *et al.*, Phys. Rev. C **74**, 024321 (2006).